ingegneria sismica
International Journal of Earthquake Engineering
Anno XLIII - Num. 2 - 2026

Construction of Intelligent Detection Model for Power Equipment Driven by Image Segmentation Algorithm

Xiaolong Chen[1], *Fang Luo*[1,*], *Qiangchao Xu*[1], *Yongbiao Liu*[1], *Jilin He*[1] *and Zhaoqi Shi*[1]

[1] Guangdong Power Grid Co., Ltd. Guangzhou Power Supply Bureau, Guangzhou, Guangdong, 510000, China

SUMMARY: *To address the issue of insufficient identification of power equipment targets in aerial images, this paper utilizes grayscale conversion technology to convert color images into grayscale images. Noise reduction is achieved by applying Gaussian filtering algorithms and bilateral filtering algorithms to images of power equipment captured during drone patrols. Next, threshold segmentation and edge detection algorithms are applied to segment the images. The segmented binary images are then processed using adaptive morphological methods to eliminate interference introduced during binarization, thereby enhancing image readability and integrity. Results show that the proposed method achieves an accuracy rate of 96.91% for image segmentation precision and a correct rate of 97.5% for overall sample detection. The method achieves a fault detection accuracy rate of over 95% for power equipment images, demonstrating good performance in detecting corrosion-related faults. Additionally, even under complex background conditions, the model achieves an accuracy rate of over 90% in fault judgment. This highlights the significant theoretical and practical significance of this method in the intelligent detection application of power equipment.*

KEYWORDS: *image grayscaling; image denoising technology; image segmentation algorithm; edge detection algorithm; power equipment*

1 Introduction

For power systems critical to national security and the safety of national production and daily life, the safe and stable operation of power systems is increasingly receiving attention. Power equipment serves as the hub and conduit of transmission and distribution grids, and during use, issues such as aging, neglect, and potential faults may arise. As power systems continue to expand and update, traditional inspection methods reliant on manual patrols and regular scheduled maintenance face challenges such as low efficiency, high rates of missed reports, and false positives [1]. In the process of intelligent grid development, intelligent technology collaborates with power systems to conduct preventive inspections, defect detection, and fault detection of power equipment, thereby improving inspection efficiency and accuracy, and playing a role in preventing and identifying potential hazards [2-4].

With the continuous advancement of technology, the introduction of intelligent technologies enables power equipment to monitor operational status in real-time through sensors and monitoring systems. By collecting, analyzing, and calculating data and images using algorithms, potential issues can be promptly identified and addressed, thereby preventing equipment failures, defects, or even accidents [5-8]. Once issues are detected, the system can automatically

*tempmail0808@163.com
https://doi.org/10.65102/is2026661
Published: 30 April, 2026

diagnose and repair faults and defects, improving the efficiency and accuracy of fault resolution. This reduces equipment failure rates, extends equipment lifespan, and significantly enhances operational efficiency and utilization rates by minimizing unnecessary downtime during production, thereby saving time and costs for enterprises [9-12].

In the inspection of electrical equipment, image-based methods are commonly used, so most research focuses on utilizing image processing techniques to improve detection accuracy and precision. Image segmentation is an important image processing technique that divides pixels in an image into distinct regions according to specific rules, enabling subsequent processing and analysis. Image segmentation algorithms include threshold-based methods, region growing methods, edge detection, clustering analysis, and deep learning algorithms. Effective and reasonable image segmentation can extract highly useful information for content-based image retrieval and object analysis, thereby enabling higher-level image understanding. This technology has widespread applications in fields such as medical image processing, autonomous driving vision, security surveillance, and automated inspection [13-17].

By incorporating intelligent technologies, power equipment can respond more accurately and swiftly in areas such as detection and diagnosis, providing critical support for modern industrial production. Ye [18] utilized optoelectronic sensor technology to capture data from power lines on utility poles and within a 100-meter radius around them, and developed an intelligent fault detection system for power equipment based on augmented reality and deep neural networks. Ding et al. [19] developed an AI-supported wind power equipment anomaly detection system, using variational modal decomposition to extract abnormal features from real-time remote monitoring videos of wind power equipment, and applying support vector machine algorithms for anomaly detection, thereby improving the timeliness and accuracy of detection. Zhang et al. [20] designed an intelligent detection model for substation equipment infrared images, using an improved YOLOv3 (You Only Look Once) algorithm for target localization and overheating fault diagnosis.

Using intelligent unmanned aerial vehicles for real-time capture of insulator images, Deng et al. [21] established an intelligent detection method for insulator faults on transmission lines using mobile edge computing and deep learning (YOLOv4), achieving an accuracy rate of 94.5% and a detection speed of 58.5 frames per second, thereby reducing system costs, drone energy consumption, and network latency issues. Lu et al. [22] developed a power equipment insulator detection method based on an improved YOLOv5s model, achieving a detection accuracy of 93.81% and a detection speed of 145.64 frames per second. Xuan et al. [23] proposed an intelligent detection method for substation equipment, primarily detecting equipment images under the YOLOv5 object detection model. The detection performance is good under conditions such as occlusion, reflection, and equipment aging, with particularly notable results for detecting minor faults. Shiling and Xiping [24] applied image processing techniques to extract and compare features from high-definition digital images, ultraviolet images, and infrared images of power equipment, combining neural networks and wavelet functions to detect equipment abnormalities and defects. Davari et al. [25] shared a method for detecting and classifying defects in power distribution lines. Each frame of the captured distribution line video is processed, using the Faster R-Convolutional Neural Network to detect defects. The frames are then segmented for corona color threshold processing and median filtering of the median image connected components, with classification performed using AlexNet or GoogleNet. Wang et al. [26] designed a field detection method for substation insulators based on instance segmentation and infrared insulator image temperature analysis, utilizing masked R-Convolutional Neural Networks, transfer learning, and dynamic learning rate algorithms.

Image segmentation algorithms range from end-to-end semantic segmentation to U-Net, incorporating attention mechanisms in Transformer segmentation models, and lightweight

segmentation networks. Hong et al. [27] proposed a distribution network feeder detection method based on semantic segmentation algorithms, overlaying feeder transient zero-sequence voltage and current onto a single image for pixel classification and segmentation, and detecting feeders based on pixel counts, achieving an accuracy rate exceeding 95% and up to 99% on complete data. Duan et al. [28] utilized transfer learning to highlight transformer fault image features, performed image segmentation using image segmentation technology to extract fault region features, and conducted feature classification and localization using a deep convolutional neural network, thereby achieving intelligent localization of internal degradation in transformers. Zhang and Zhu [29] improved the ASPP module in the encoder of the segmentation network, incorporated an attention mechanism into the network, and added a structured feature enhancement module in the decoder, forming the CS_DeeplabV3+ segmentation network model, which improved the accuracy of infrared image segmentation for power equipment defects. Hou et al. [30] designed a lightweight DeepLabv3+ segmentation model and combined it with a feature pyramid structure to segment oil leakage images of oil-filled equipment in substations, optimizing the accuracy of image region and edge segmentation and promoting accurate detection of equipment oil leakage. Zou et al. [31] introduced a skip connection module, wavelet convolution, and an adaptive attention mechanism to improve the traditional U-Net segmentation algorithm, achieving a segmentation algorithm with higher accuracy for real-time detection systems in substations. Zhao et al. [32] developed an infrared thermal image instance segmentation method to address the issues of low accuracy and false detection in substation equipment instance segmentation. This method was realized through the integration of power industry expertise, visual feature inference, residual networks, and feature fusion pyramids. In Fambrini et al.'s [33] experimental tests, the JSEG segmentation algorithm was used to segment thermal imaging images of power distribution networks, combining deep learning neural networks to identify segmentation features, thereby replacing manual inspections of power distribution networks. Qi et al. [34] addressed noise and background interference issues in infrared image segmentation of substation electrical equipment using a multi-information fusion fuzzy clustering method, which also improved segmentation accuracy. Liu et al. [35] optimized an infrared image segmentation method based on the maximum interclass variance threshold using the gray wolf optimization algorithm to accelerate segmentation speed, and improved infrared image temperature feature extraction using the k-nearest neighbor algorithm. Takeuchi et al. [36] compared the performance of various image segmentation methods in segmenting thermal imaging images of substations. Threshold-based methods are fast but prone to over-segmentation, with lower segmentation accuracy and precision than clustering-based methods. The fuzzy C-means clustering method performed best.

In the process of constructing an intelligent detection model for power equipment, this paper first uses image grayscaling to convert color three-channel images into single-channel grayscale images, thereby reducing the amount of data that needs to be processed. An improved filtering algorithm is then used to remove noise from aerial images and enhance the details of useful parts of the image. Based on threshold segmentation and image edge detection techniques, a morphological-based image recognition and detection algorithm for power equipment defects is proposed. This algorithm highlights the boundaries and shape features of the target area, thereby enhancing the contrast of the target boundary region and eliminating interference caused during the binarization process of intelligent power equipment detection. The segmentation performance and detection efficiency of the model are analyzed. Finally, using common power equipment faults encountered during drone patrols as examples, the effectiveness of intelligent power equipment detection is analyzed.

2 Intelligent detection model for power equipment based on image segmentation algorithms

2.1 Image Preprocessing Technology

2.1.1 Image grayscaling

All images of power equipment captured by drones are color images, where the color of each pixel is determined by the three channels R, G, B. Each component has 256 possible values, resulting in over 16 million possible color variations per pixel. The process of converting a color image into a grayscale image is called image grayscaling. A grayscale image is a special type of color image where the R, G, B components are all the same. Each pixel has 256 possible values, with a grayscale range of 0 to 255. After grayscaling, the amount of data required for processing is significantly reduced. Since color images contain a large amount of data, but the majority of features of the target objects in the image do not necessarily require detailed color data, digital image processing often focuses on grayscale images.

The grayscale conversion process may lose some detail information, but its impact on subsequent target extraction and foreign object detection is minimal and can be largely ignored. The grayscale conversion process can be achieved using two methods. The first involves calculating the average of the R, G, B components for each pixel and using this value as the grayscale level. The second method uses the Y component in the YUV color space to represent the grayscale level, with the formula for this component being:

$$Y = 0.297R + 0.585G + 0.115B \tag{1}$$

2.1.2 Image Denoising

(1) An improved adaptive median filter algorithm

A commonly used and effective method for removing salt-and-pepper noise is the median filter algorithm, whose basic principle is as follows: first, determine a window template of a certain shape and size; then, statistically sort the gray values of all pixels within the window; finally, replace the gray value of the pixel at the center of the window with the median value of the sorted sequence. Let $g(x, y)$ denote the original gray-level value of the central pixel, $f(x, y)$ denote the gray-level value of the pixel after median filtering, and A denote the window template. Then the median filter can be expressed as:

$$f(x, y) = \underset{(k,l)\in A}{Med} g(x-k, y-l) \tag{2}$$

The algorithm flow of traditional median filtering is as follows:

a) Determine the shape and size of the window template, which is generally a 3×3 rectangular area;

b) Use this template to iterate through the image pixels one by one, extract the gray values of all pixels within the window, and sort them statistically;

c) Take the median of the gray value sequence and replace the gray value of the pixel at the center of the window with this value.

(2) Gaussian filtering algorithm

In image denoising, Gaussian filtering [37] is often used to eliminate Gaussian noise. Its basic principle is as follows: determine a window template of a certain shape and size, and calculate the gray value of the pixel at the center of the template by taking the weighted average

of its own gray value and the gray values of all pixels in its neighborhood. Gaussian filtering differs from general smoothing filtering in that, when averaging the gray values within the neighborhood, pixels at different positions have different weights, with those closer to the center of the template having higher weights. This allows Gaussian filtering to preserve more of the overall gray value distribution characteristics of the image.

The form of the two-dimensional Gaussian function is:

$$h(x,y)=\frac{1}{2\pi\sigma^2}e^{-\frac{x^2+y^2}{2\sigma^2}} \tag{3}$$

where (x,y) is any point on the function, and σ is the standard deviation. The specific approach of Gaussian filtering is as follows: discretize the two-dimensional Gaussian function, use the Gaussian function values at the discrete points as weights, and perform weighted averaging on each pixel value in the grayscale matrix collected by the window template to achieve the purpose of eliminating Gaussian noise. Assuming the size of the window template is $(2k+1)\times(2k+1)$, the template coefficient for each element in the template can be calculated using the following formula:

$$H_{i,j}=\frac{1}{2\pi\sigma^2}e^{-\frac{(i-k-1)^2+(j-k-1)^2}{2\sigma^2}} \tag{4}$$

where $(i,j)(i,j=1,2,\cdots,2k+1)$ represents the relative coordinates of each pixel point within the window template.

(3) Bilateral filtering algorithm

Bilateral filtering is based on Gaussian filtering and primarily improves upon the direct convolution of Gaussian weight coefficients with image information in Gaussian filtering. It first optimizes the weight coefficients into the product of Gaussian function values and image brightness information, then performs convolution between the optimized weight coefficients and image information. This allows the algorithm to consider edge information in the image during filtering, thereby preserving the clarity of edge information that would otherwise become blurred after traditional Gaussian filtering.

In a bilateral filter, the output pixel value depends on the weighted combination of neighboring pixel values. The algorithm's implementation principle is as follows: Let (i,j) be the central pixel point, and (k,l) be the neighboring pixels of this pixel point. After bilateral filtering, the output pixel value becomes:

$$g(i,j)=\frac{\sum_{(k,l)\in Si,j} f(k,l)\omega(i,j,k,l)}{\sum_{(k,l)\in Si,j}\omega(i,j,k,l)} \tag{5}$$

Here, Si,j denotes the rectangular window template containing the central pixel point (i,j), with a size of $(2N+1)\times(2N+1)$. The right-hand side of the equation represents the weighted average of the pixel values within the neighborhood of the central pixel point. The weighting coefficient $\omega(i,j,k,l)$ depends on the product of the spatial domain kernel and the pixel range domain kernel, which can be expressed as:

$$d(i,j,k,l)=\exp(-\frac{(i-k)^2+(j-l)^2}{2\sigma_d^2}) \tag{6}$$

$$r(i,j,k,l)=\exp(-\frac{\| f(i,j)-f(k,l)\|^2}{2\sigma_r^2}) \tag{7}$$

where σ_d and σ_r represent the smoothing parameters for the spatial domain and pixel range domain, respectively, and $f(i,j)$ and $f(k,l)$ represent pixel values. Multiplying equations (6) and (7) yields the weighting coefficients:

$$\omega(i,j,k,l)=\exp(-\frac{(i-k)^2+(j-l)^2}{2\sigma_d^2}-\frac{\| f(i,j)-f(k,l)\|^2}{2\sigma_r^2}) \tag{8}$$

2.2 Image segmentation technology

2.2.1 Threshold-based segmentation methods

Threshold segmentation is a region-based image segmentation technique. Let $I(x,y)$ be a grayscale image with M×N pixels, where x,y are the two-dimensional coordinates in the image, and T is the set threshold. The grayscale image before transformation is $f(x,y)$, and the binary image after transformation is $g(x,y)$. The formula for the threshold binary transformation of the image is:

$$g(x,y)=\begin{cases}255 & f(x,y)\geq \mathrm{T}\\ 0 & f(x,y)<\mathrm{T}\end{cases} \tag{9}$$

In the formula, 255 is used so that the entire image can be easily displayed with a clear black-and-white effect in the experiment.

The following is an introduction to three automatic threshold segmentation methods: iterative threshold selection method, Otsu method, and maximum entropy threshold method.

(1) Iterative Threshold Selection Method

This method is based on the concept of approximation. The steps for obtaining the iterative threshold can be summarized as follows:

a) Determine an initial threshold $T(j)$, where j is the iteration count, with $j=0$ initially.

b) Use $T(j)$ to segment the image into two regions $C_1^{(j)}$ and $C_2^{(j)}$.

c) Calculate the average gray values of the two regions:

$$u_1^{(j)}=\frac{1}{N_1^{(j)}}\sum_{f(x,y)\in C_1^{(j)}} f(x,y) \tag{10}$$

$$u_2^{(j)}=\frac{1}{N_2^{(j)}}\sum_{f(x,y)\in C_2^{(j)}} f(x,y) \tag{11}$$

In the equation, $N_1^{(j)}, N_2^{(j)}$ are the number of pixels in regions C_1 and C_2 at the jth iteration; $f(x, y)$ is the grayscale value of point (x, y) in the image.

d) Then calculate the new threshold value, i.e.:

$$T(j+1) = \frac{u_1^{(j)} + u_2^{(j)}}{2} \tag{12}$$

e) Set $j = j+1$, repeat steps ② to ④ until the difference between $T(j+1)$ and $T(j)$ is less than a predetermined value.

(2) Otsu's method

Otsu's method uses a hypothetical gray value t to divide the gray values of an image into two groups. When the interclass variance between these two groups is maximized, the gray value t is the optimal threshold for segmentation.

Let an image have M gray values, and the gray value t take values between 0 and M-1. the image is divided into two groups G_0 and G_1 using this gray value t, with pixel gray values ranging from 0 to t and t+1 to M-1, respectively. Let N denote the total number of pixels, and N_i denote the number of pixels with gray value i. The probability of each gray value i occurring is $p_i = n_i / N$; Assume that the percentages of pixels in groups G_0 and G_1 in the entire image are ω_0 and ω_1, respectively, and the average gray values of the two groups are u_0 and u_1, respectively.

Probability:

$$\omega_0 = \sum_{i=0}^{t} p_i \tag{13}$$

$$\omega_1 = \sum_{i=t+1}^{M-1} p_i = 1 - \omega_0 \tag{14}$$

Average gray value:

$$u_0 = \sum_{i=0}^{t} i p_i \tag{15}$$

$$u_1 = \sum_{i=t+1}^{M-1} i p_i \tag{16}$$

The total average gray value of the image is:

$$u = \omega_0 \times u_0 + \omega_1 \times u_1 \tag{17}$$

The interclass variance is:

$$g(t) = \omega_0 (u_0 - u)^2 + \omega_1 (u_1 - u)^2 = \omega_0 \omega_1 (u_0 - u_1)^2 \tag{18}$$

The optimal threshold is:

$$T = argmax(g(t)) \tag{19}$$

Even when the t-value corresponding to the maximum interclass variance is obtained.

(3) Maximum Entropy Threshold Method

The maximum entropy threshold method determines the optimal threshold for binarization by calculating the entropy of the grayscale histogram of the test image.

Assuming that the grayscale range of an image is $0,1,2,\cdots,M-1$, the entropy of its corresponding histogram can be defined as:

$$H = -\sum_{i=0}^{M-1} p_i \ln p_i \tag{20}$$

In the formula, p_i is the probability that a pixel with grayscale value i appears in the entire image.

If the image is divided into two parts, the target and the background, using a threshold t, and they are designated as the O zone and the B zone, respectively, their probability distributions are as follows:

O zone:

$$\frac{p_i}{p_t}, i = 0,1,\cdots,t, \text{Of which} p_t = \sum_{i=0}^{t} p_i \tag{21}$$

Zone B:

$$\frac{p_i}{1-p_i}, i = t+1,\cdots,M-1 \tag{22}$$

Order:

$$H_t = -\sum_{i=0}^{t} p_i \ln p_t \tag{23}$$

$$H = -\sum_{i=0}^{M-1} p_i \ln p_i \tag{24}$$

Then, the entropy functions of target O and background B are respectively:

$$H_O(t) = -\sum_{i=0}^{t} \frac{p_i}{p_t} \ln \frac{p_i}{p_t} = \ln p_t + \frac{H_t}{p_t} \tag{25}$$

$$H_B(t) = -\sum_{i=0}^{t} \frac{p_i}{1-p_t} \ln \frac{p_i}{1-p_t} = \ln(1-p_t) + \frac{H-H_t}{1-p_t} \tag{26}$$

The total entropy of the image is:

$$H(t) = H_O(t) + H_B(t) = \ln p_t(1-p_t) + \frac{H_t}{p_t} + \frac{H - H_t}{1-p_t} \tag{27}$$

The optimal threshold T is the value that maximizes the total entropy of the image, expressed as:

$$T = argmax(H(t)) \tag{28}$$

2.2.2 Edge-based segmentation methods

The gradient algorithm, which uses the first and second derivatives at the edges of an image to find extrema, has become a classic algorithm for edge detection [38].

The gradient operator is the operator of the first derivative. Typically, for a continuous function $f(x,y)$, its gradient at (x,y) can be represented as a vector $G(x,y)$, where the direction of $G(x,y)$ corresponds to the direction of the maximum rate of change of $f(x,y)$ when it increases:

$$G(x,y) = \begin{bmatrix} G_x \\ G_y \end{bmatrix} = \begin{bmatrix} \frac{\partial f}{\partial x} \\ \frac{\partial f}{\partial y} \end{bmatrix} \tag{29}$$

The magnitude of the gradient is:

$$|G(x,y)| = \sqrt{G_x^2 + G_y^2} = \sqrt{(\frac{\partial f}{\partial x})^2 + (\frac{\partial f}{\partial y})^2} \tag{30}$$

In practical applications, the absolute value is used to approximate the gradient amplitude, i.e.:

$$|G(x,y)| = |G_x| + |G_y| = |\frac{\partial f}{\partial x}| + |\frac{\partial f}{\partial y}| \tag{31}$$

Another simple method is to use the chessboard distance, which is:

$$|G(x,y)| \approx max(|G_x|, |G_y|) = max(|\frac{\partial f}{\partial x}|, |\frac{\partial f}{\partial y}|) \tag{32}$$

Let $\theta(x,y)$ denote the direction angle of vector $G(x,y)$ at (x,y). The direction of the gradient is defined as:

$$\theta(x,y) = arctan(\frac{G_y}{G_x}) \tag{33}$$

In the formula, θ is the angle relative to the x axis.

Several commonly used classical edge detection methods are as follows:

(1) Roberts operator

The Roberts operator uses a local difference operator to find edges. Let $f(x,y)$ be the input image and $G(x,y)$ be the output image, then:

$$G(x,y)=\sqrt{(\sqrt{f(x,y)}-\sqrt{f(x+1,y+1)})^2+(\sqrt{f(x+1,y)}-\sqrt{f(x,y+1)})^2} \tag{34}$$

The template format is as follows:

$$G_x=\begin{bmatrix}1 & 0\\ 0 & -1\end{bmatrix}\quad G_y=\begin{bmatrix}0 & 1\\ 0-1 & 0\end{bmatrix} \tag{35}$$

(2) Sobel operator

The Sobel operator consists of two sets of 3×3 matrices. After convolving it with the image, the approximate brightness difference in these two directions can be obtained. G_x and G_y represent the images detected by horizontal and vertical edges, respectively. The template form is:

$$G_x=\begin{bmatrix}-1 & 0 & 1\\ -2 & 0 & 2\\ -1 & 0 & 1\end{bmatrix}\quad G_y=\begin{bmatrix}-1 & -2 & -1\\ 0 & 0 & 0\\ 1 & 2 & 1\end{bmatrix} \tag{36}$$

The sum of the template coefficients is 0. At this point, the corresponding template is 0 in the area where the grayscale value remains unchanged. The specific convolution algorithm is as follows:

$$\begin{aligned}G_x=&f(x+1,y-1)+2f(x+1,y)+f(x+1,y+1)\\&-f(x-1,y-1)-2f(x-1,y)-f(x-1,y+1)\end{aligned} \tag{37}$$

$$\begin{aligned}G_y=&f(x-1,y+1)+2f(x,y+1)+f(x+1,y+1)\\&-f(x-1,y-1)-2f(x,y-1)-f(x+1,y-1)\end{aligned} \tag{38}$$

Among them, $f(x,y)$ is the grayscale value of the image at point (x,y).

Then the gradient magnitude is:

$$G(x,y)=\sqrt{G_x^2+G_y^2} \tag{39}$$

(3) Laplace operator

The Laplace transform of a two-dimensional image is an isotropic second-order derivative, defined as:

$$\nabla^2 f=\frac{\partial^2 f}{\partial x^2}+\frac{\partial^2 f}{\partial y^2} \tag{40}$$

Its second-order partial derivative is:

$$\begin{aligned}\frac{\partial^2 f(x,y)}{\partial x^2} &= \Delta_x f(x+1,y) - \Delta_x f(x,y) \\ &= f(x+1,y) + f(x-1,y) - 2f(x,y)\end{aligned} \tag{41}$$

$$\begin{aligned}\frac{\partial^2 f(x,y)}{\partial y^2} &= \Delta_y f(x,y+1) - \Delta_y f(x,y) \\ &= f(x,y+1) + f(x,y-1) - 2f(x,y)\end{aligned} \tag{42}$$

Therefore, the Laplace operator is defined as:

$$\begin{aligned}\nabla^2 f &= \frac{\partial^2 f}{\partial x^2} + \frac{\partial^2 f}{\partial y^2} \\ &= f(x+1,y) + f(x-1,y) \\ &+ f(x,y+1) + f(x,y-1) - 4f(x,y)\end{aligned} \tag{43}$$

The Laplace operator is not typically used directly for edge detection because it is very sensitive to image noise.

The commonly used Laplace operator template is:

$$H_1 = \begin{bmatrix} 0 & -1 & 0 \\ -1 & 4 & -1 \\ 0 & -1 & 0 \end{bmatrix} \quad H_2 = \begin{bmatrix} -1 & -1 & -1 \\ -1 & 8 & -1 \\ -1 & -1 & -1 \end{bmatrix} \tag{44}$$

(4) Gauss-Laplace Operator

The Gauss-Laplace operator effectively reduces sensitivity to image noise and enhances robustness. Its essence is as follows: first, apply Gaussian blurring to the image, then calculate the second-order derivative, and finally determine whether it is an image edge by identifying the pixels corresponding to points where the second-order derivative is zero. A commonly used 5×5 Gauss-Laplace operator template is:

$$\begin{bmatrix} -2 & -4 & -4 & -4 & -2 \\ -4 & 0 & 8 & 0 & -4 \\ -4 & 8 & 24 & 8 & -4 \\ -4 & 0 & 8 & 0 & -4 \\ -2 & -4 & -4 & -4 & -2 \end{bmatrix} \tag{45}$$

2.2.3 Region-based segmentation methods

Image region segmentation refers to dividing an image into regions, extracting the desired image data segments for further processing, and discarding the remaining unnecessary image data. The primary purpose of region segmentation is to reduce the data volume for subsequent image processing. Among the various region segmentation algorithms available, the region growing method is currently the most widely used. The advantages of this algorithm include relatively simple computation, making it suitable for small-area segmentation. However, it has the drawback of requiring predefined seed points and being highly sensitive to noise or outliers, which may result in gaps in the segmentation. Additionally, since it is a serial computation

method, the computation speed becomes relatively slow when segmenting images with larger region areas.

2.3 Intelligent detection model for power equipment driven by image segmentation algorithms

2.3.1 Power image segmentation technology based on adaptive morphology

Morphological processing of images primarily targets binary images obtained after threshold segmentation. By expanding or searching the target region, the boundaries and shape characteristics of the target region are highlighted, thereby enhancing the contrast of the target boundary region and eliminating interference introduced during the binarization process. To improve the readability of power equipment images during the detection process while preserving the integrity of the image's feature information, the first step in image detection should be to remove the impact of irrelevant noise on the results, followed by morphological processing of the binarized results. The purpose of this is to reduce the size of the target region in the image, causing the edges of the detection results to contract to some extent, and eliminating small and insignificant target interferences. Taking insulators as an example, the effect diagram of the corrosion operation is shown in Figure 1, where (a) is the image to be processed, (b) is the structural element, and (c) is the result of the corrosion image.

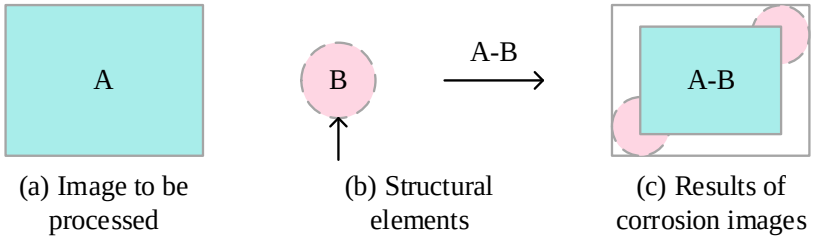

Figure 1: An effect diagram of the corrosion treatment

The corrosion operator is "-", which means the following:

$$A-B=\{x\,|\,B_x\subseteq A\} \tag{46}$$

The above equation performs a erosion operation on a binary image by taking the intersection of template B and image A, and the intersection area is entirely within the area of image A. By sliding B, all erosion results that satisfy the conditions are obtained, as shown in Figure 2, where (a) is the image to be processed, (b) is the structural element, and (c) is the result of the dilation image.

The dilation operator is "$\oplus$", which is represented as follows:

$$A\oplus B=\{x\,|\,B\cap A\neq\Theta\} \tag{47}$$

The above equation shows that B is used to expand image A, where B is a convolution template or convolution kernel, and its shape is elliptical.

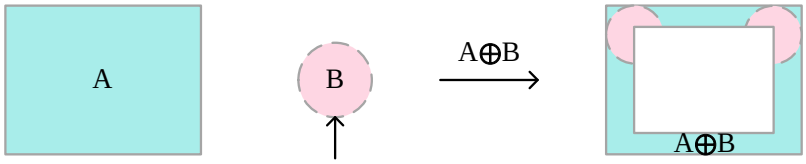

(a) Image to be processed (b) Structural elements (c) Results of expanded images

Figure 2: An effect diagram of the expansion operation

Without altering the area of the binary image after segmentation, further operations are performed on the binary image processed by morphological operations to eliminate small, isolated pixels in the binary image, thereby achieving the goal of smoothing the target boundary shape. For the binary image of the insulator, erosion followed by dilation operations are performed, i.e., the opening operation. For power equipment images, dilation is performed first, followed by erosion, known as the closing operation, to fill small voids within the segmented image. The expressions for the opening and closing operations are as follows:

$$A \circ B = (A - B) \oplus B \tag{48}$$

$$A \bullet B = (A + B) - B \tag{49}$$

2.3.2 Power Equipment Location

First, most of the interfering colors in the background of the power equipment image are removed. Then, morphological processing is used to retain the parts of the power equipment that are relevant to defect detection. Finally, the areas within the connected regions are calculated, and small areas within the connected regions of the candidate regions are eliminated, so that the image to be segmented is clearly highlighted. The flowchart for power equipment localization is shown in Figure 3.

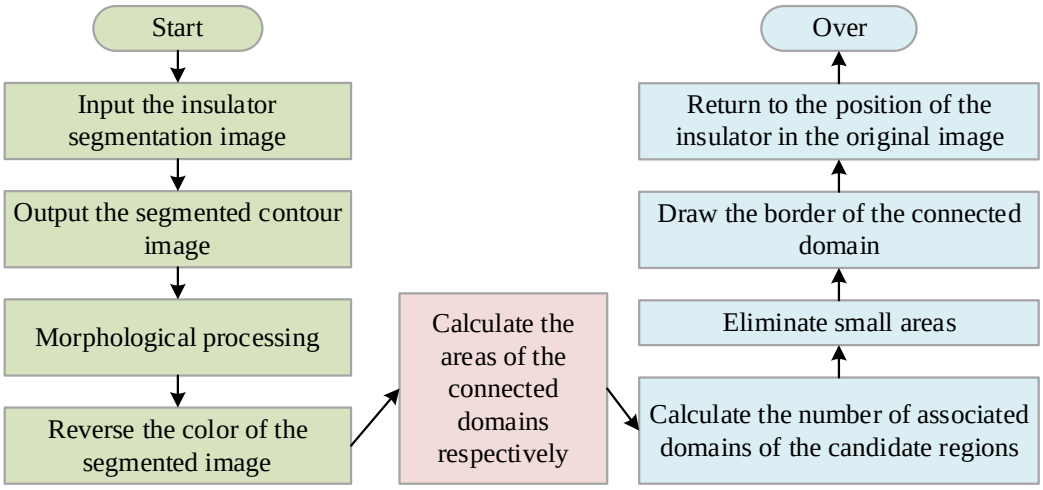

Figure 3: Implementation flow chart for power equipment positioning

3 Intelligent detection results of power equipment driven by image segmentation algorithms

The experimental test image database used in this paper was provided by the Research Institute

of the C City Power Bureau. All test images are real-world images of power equipment captured using drones equipped with digital cameras during on-site inspections of power systems. Images of transmission lines at different voltage levels were collected, including 180 kV, 450 kV, and 750 kV transmission lines, as experimental test images. The image acquisition device used was the HC-X900M model digital camera, with the digital image format being JPEG. The test sample database contains a total of 1,000 images. This paper randomly selected 200 test images, including 95 fault images and 105 non-fault images.

3.1 Model Performance Analysis

During the experiment, the insulator was used to split the dataset for training. The experimental hardware configuration and environment were the same as those in Chapter 3. The PyTorch deep learning framework was still used, with the following training parameter settings: batch size of 1, 150 iterations, weight decay of 0.999, and learning rate of 0.001. During training, the parameters of the network model were optimized using the mini-batch gradient descent method. During training, it is essential to minimize training time while ensuring rapid model convergence and keeping error fluctuations within a reasonable range. After multiple trials, the batch size for each training session was set to 1, and the model was trained for a total of 150 epochs.

3.1.1 Image segmentation performance

After model training is complete, data information is obtained from the training log and plotted. The loss changes in the insulator segmentation model training results are shown in Figure 4. The results show that when the number of iterations of the model reaches 31, the learning rate of the model reaches 0.001, indicating that the model is highly efficient in power equipment image segmentation.

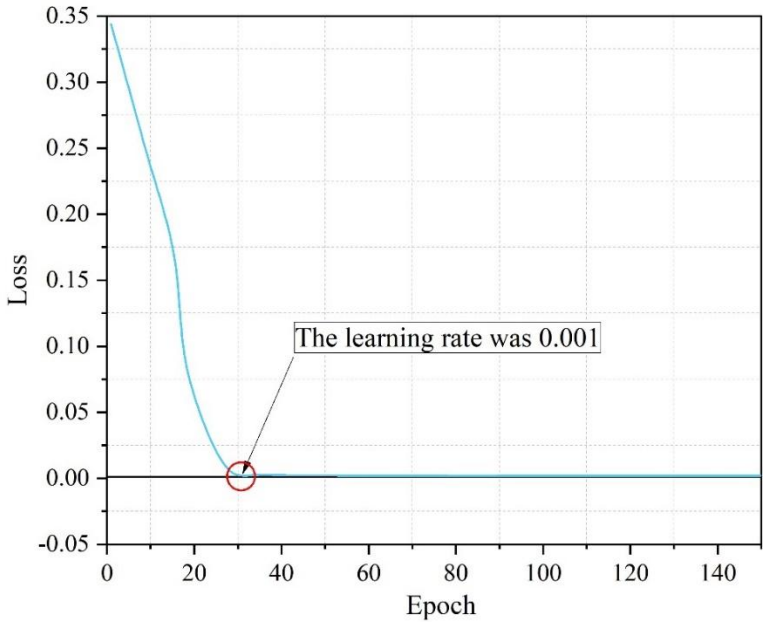

Figure 4: Loss variation of insulation partition model training results

To evaluate the segmentation performance of the proposed algorithm compared to other algorithms, we compared the proposed algorithm with the commonly used U-Net and DeeplabV3+ semantic segmentation algorithms. The comparison was conducted on the same dataset, ensuring that each algorithm achieved its optimal segmentation performance. In image

segmentation tasks, there are numerous metrics used to assess segmentation performance, among which the Mean Intersection over Union (MIoU) is the most commonly used and representative evaluation metric for measuring image segmentation accuracy.

The segmentation results of different algorithms are compared in Figure 5. It can be seen that the average MIoU value of the method proposed in this paper is 96.91%, which is 34.22% and 28.77% higher than the MIoU values of the U-Net and DeeplabV3+ segmentation algorithms, respectively. This indicates that the method proposed in this paper has greatly improved the segmentation accuracy in the task of power equipment image segmentation. As such, the algorithm proposed in this paper can effectively segment the contour features of insulators, reducing or eliminating blurred image edges, significantly accelerating training time, and achieving excellent results even under limited computer hardware resources.

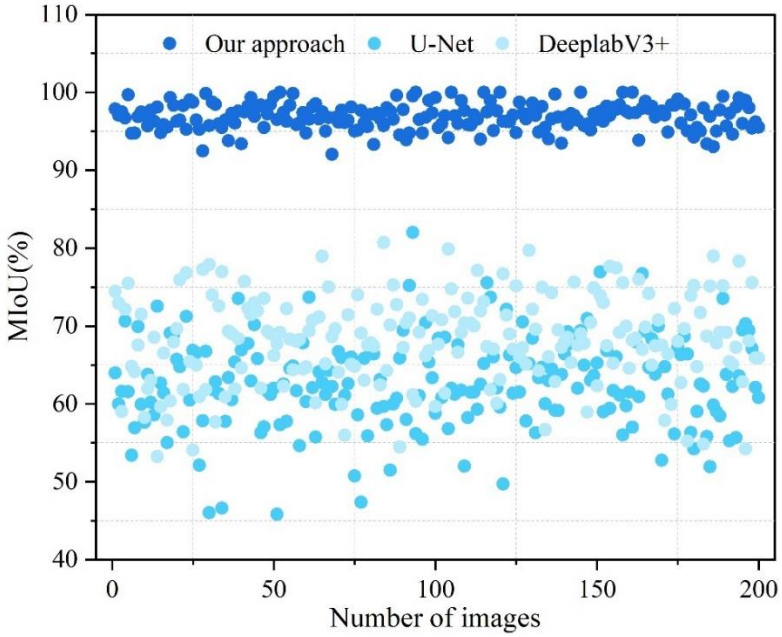

Figure 5: Comparison of results of different algorithms

3.1.2 Image detection detection results

To validate the detection effectiveness of the network model defect detection process described in this paper, 100 aerial images of normal insulators and 100 aerial images of defective insulators were selected for experimental verification under the same experimental conditions. The experimental results were evaluated using the overall sample accuracy rate as the metric. The insulator defect detection results are shown in Figure 6. As can be seen, out of 100 images of normal insulators, 100 were detected correctly and 0 were detected incorrectly, resulting in a detection accuracy rate of 100%; out of 100 images of defective insulators, 95 were detected correctly and 5 were detected incorrectly, resulting in a detection accuracy rate of 95%; the overall detection accuracy rate for the total sample was 97.5%.

Additionally, from the detection results, it can be seen that the detection accuracy rate of the algorithm for defective power equipment images is 5% lower than that for normal power equipment images. This may be due to the defects in the insulators being less prominent in aerial images. When segmenting insulators in images, the algorithm was unable to completely segment the defective parts of insulators due to interference from factors such as insulator angle and background noise. As a result, the model misclassified images containing defective insulators as normal power equipment images. However, the overall detection results indicate that the detection performance of the insulator defect detection model proposed in this paper

has met the experimental expectations.

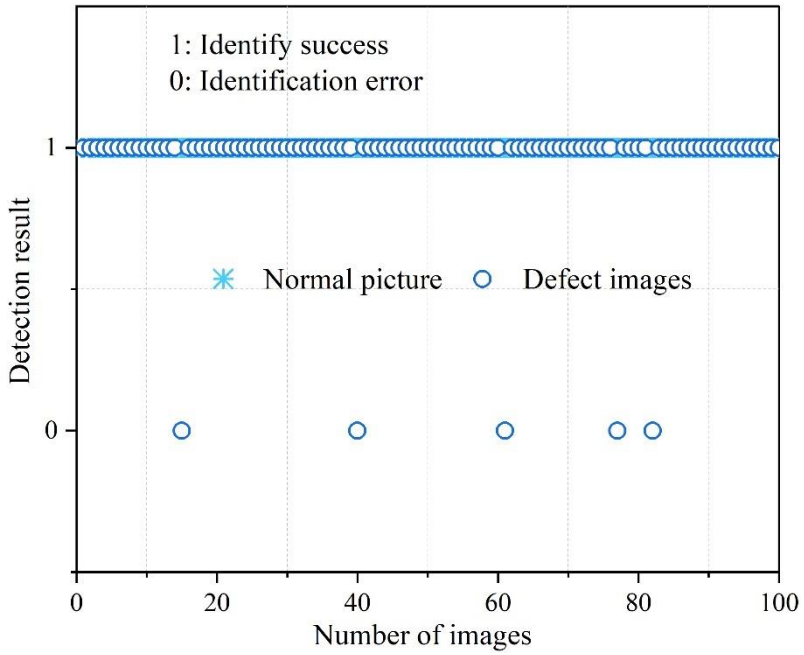

Figure 6: Insulator defect detection results

3.2 Application case of power equipment fault status judgment

This section uses common corrosion faults in electrical equipment hardware during drone line inspections as an example. The experimental test image database was provided by the C City Electric Power Bureau Research Institute. The image acquisition device was an HC-X900M digital camera, and the digital image format was JPEG. The test sample database contained a total of 200 test images, including 95 images of hardware corrosion faults and 105 images of non-corrosion faults.

3.2.1 Analysis of the results of the metal fitting corrosion failure experiment

Power equipment contains various types of metal components, and corrosion-related failures in different components exhibit distinct spatial distribution characteristics. The number of test images for each fault type is shown in Table 1. For each corrosion fault test image, there are often multiple corrosion areas. The ability to accurately identify and label all corrosion areas is an important metric for evaluating fault detection algorithms. For each test image, the number of corrosion areas contained in the image is determined using manual identification methods, serving as a basis for assessing the accuracy of the detection algorithm.

Table 1: Number of test images for various fault types

Type of corrosion failure	Number of test images (copies)
Ground wire corrosion	28
Shock absorber corrosion	13
Erosion of tower hardware	54
Non-corrosive images	105
Amount to	200

Simultaneously introduce the true positive rate (α), false negative rate (β), and number of false positives (S) as evaluation metrics to quantitatively evaluate the rust detection algorithm. Assuming that the test image contains N targets to be detected, after processing by the detection algorithm, a total of M targets are detected, among which the number of detected true targets is R, the number of undetected true targets is $R^{'}$, and the number of detected false targets is S. Then, the true positive rate (α) and false negative rate (β) are as follows:

$$\alpha = \frac{R}{N}; \beta = \frac{R^{'}}{N} \tag{50}$$

The results of the rust corrosion fault sample detection are shown in Table 2. Through manual identification, a total of 234 target rust corrosion areas were found in 95 rust corrosion fault images. Using the rust corrosion fault detection algorithm proposed in this paper for fault detection, a total of 231 true rust corrosion areas were detected, with 2 missed detections and 1 false detection of a rust corrosion area. Based on data statistical theory, the evaluation metrics for the corrosion detection algorithm proposed in this paper are as follows: the average number of false positives per image is 0.01, the false negative rate is 2.04%, and the true positive rate is 97.96%. This algorithm demonstrates excellent corrosion fault detection performance, effectively detecting and identifying the majority of corrosion regions with an extremely low false negative rate. It is evident that the algorithm proposed in this paper exhibits exceptional robustness.

Table 2: Test results of some rusted fault samples

Sample number	Actual target number (number)	Number of test targets (individuals)	Number of false detections S (number)	Loss β(%)	Detection rate α(%)
1	4	4	0	0	100
2	6	6	0	0	100
3	5	4	1	20	80
4	5	5	0	0	100
5	4	4	0	0	100
6	6	5	1	16.67	83.33
7	3	3	0	0	100
8	5	5	0	0	100
9	6	7	1	0	100
10	5	5	0	0	100
Amount to	49	48	1	2.04	97.96

3.2.2 Analysis of the time required to identify metal hardware corrosion faults

For the rust corrosion fault detection algorithm proposed in this paper, in addition to the algorithm's detection accuracy, the algorithm's computational speed is also an important evaluation criterion. This paper implements the relevant algorithms for rust corrosion fault detection using the C++ language on the VS compilation platform. Independent algorithm runtime tests were conducted for each component of the complete detection system. The test environment featured an Intel i3-4130 3.40GHz CPU and 6.00GB of RAM. The test images were uniformly set to 1080×1080 resolution, and 100 test images were selected for algorithm

speed testing. The time complexity analysis of the rust identification algorithm is shown in Table 3. Based on the above runtime test data, the rust defect detection algorithm proposed in this paper demonstrates relatively fast runtime speed and strong timeliness under the current test environment.

Table 3: Analysis of time complexity of rust identification algorithm

Algorithm	Time (seconds)
Rust image differentiation	0.8148
Improve the ultra-green method	0.1447
image preprocessing	1.5286
image segmentation	0.2491
Morphological treatment	1.7453
Rust marks	3.9311
Amount to	8.4136

3.2.3 Analysis of the results of insulator damage fault diagnosis

To accurately extract the insulator region from the original image, it is necessary to filter the connected regions in the segmented binary image to avoid interference from other incorrectly segmented connected regions in the subsequent fault state judgment.

In the binary image, each connected region is traversed sequentially. For each connected region, the spatial coordinates of the extreme values are statistically analyzed using row-by-row and column-by-column scanning methods to determine the position of each connected region in the original image, and these regions are marked in red in the image. The insulator binary image and connected region identification and screening results are shown in Figure 7, where (a) is the connected region identification, and (b) is the insulator binary image screening result.

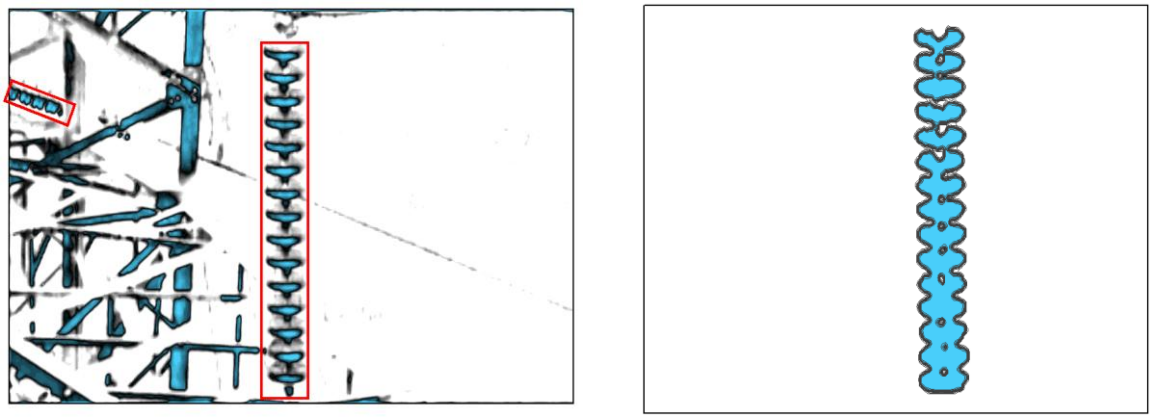

(a) Connect area identifiers

(b) Filtering results of binary image of insulator

Figure 7: Identification and screening results of binary image areas of insulators

After obtaining the pixel points of the insulator edge contour, the spatial coordinates of the corresponding pixel points on the left and right contours are statistically represented using a curve diagram, with the horizontal axis representing the major axis coordinate of the insulator region and the vertical axis representing the minor axis coordinate. Figure 8 shows the complete contour curve of the insulator edge, where (a) and (b) represent the contour curves of the left and right edges, respectively. As shown in the figure, the two sides of the complete insulator

exhibit a regular spatial arrangement, with the curve diagram displaying periodic characteristics. The alternating peaks and valleys represent the convex and concave arrangement of the insulator edge. The spatial coordinate variation rate of the complete insulator edge pixels exhibits a distinct periodicity. However, when the insulator experiences a failure, the coordinates of the edge pixels at the failure location undergo a sudden change, resulting in an isolated spatial distribution.

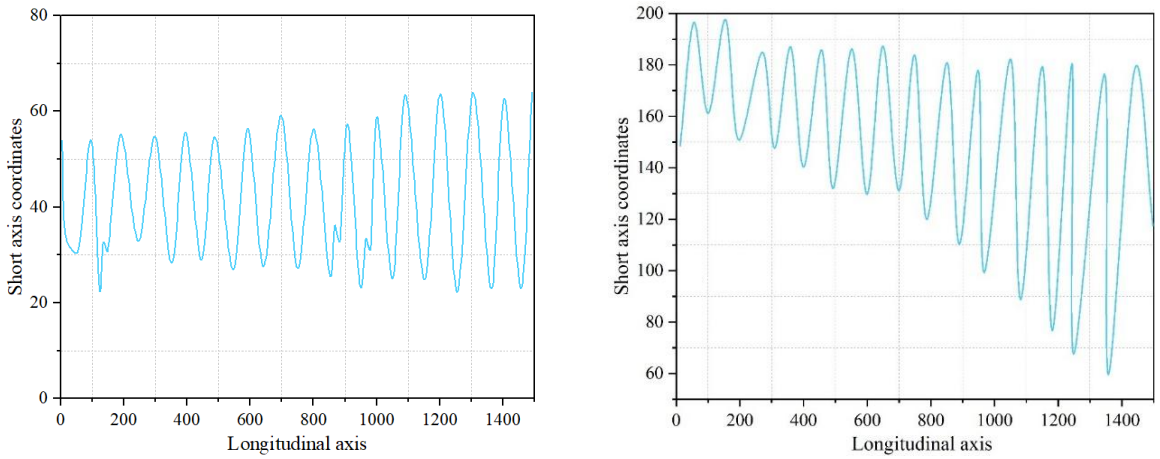

(a) The left edge contour curve (b) The contour curve on the right edge

Figure 8: Complete insulator edge contour curve

The experimental test image data used in this paper includes 117 images of damaged electrical equipment and 83 images of intact electrical equipment. In the test image database used in this paper, some of the electrical equipment images contain complex background environments, including green vegetation. The classification of insulator test images is shown in Table 4.

Table 4: Insulator test image classification

Image type	Image of damaged insulator (frame)	Complete insulator image (frame)
Single background	64	41
Complex background	53	42
Amount to	117	83

This paper conducts fault detection algorithm tests on images of power equipment under different background conditions and analyzes and compares the final insulator status detection results with manual judgment results to determine the accuracy of the fault status detection algorithm, quantifying the evaluation through recognition rates. Figure 9 shows the statistical results of insulator fault detection, where A: single background with defects, B: complex background with defects, C: single background without defects, D: complex background without defects; The numbers in the figure represent the number of test samples, with 1 indicating correct identification and 0 indicating incorrect identification. Based on the above statistical data, the insulator fault detection algorithm proposed in this paper demonstrates good detection performance, achieving a fault detection rate of 93.5% for insulator damage, and effectively detecting and identifying most insulator fault areas. Additionally, for insulator test images significantly affected by external factors such as lighting conditions, aerial photography translation and rotation transformations, and noise, after applying corresponding image

preprocessing, insulator segmentation, and fault judgment operations, the algorithm proposed in this paper still achieves a high detection rate for insulator damage faults, demonstrating strong robustness. Compared to traditional insulator detection algorithms, it offers significant advantages and holds important theoretical and practical significance for unmanned aerial vehicle (UAV) inspection applications.

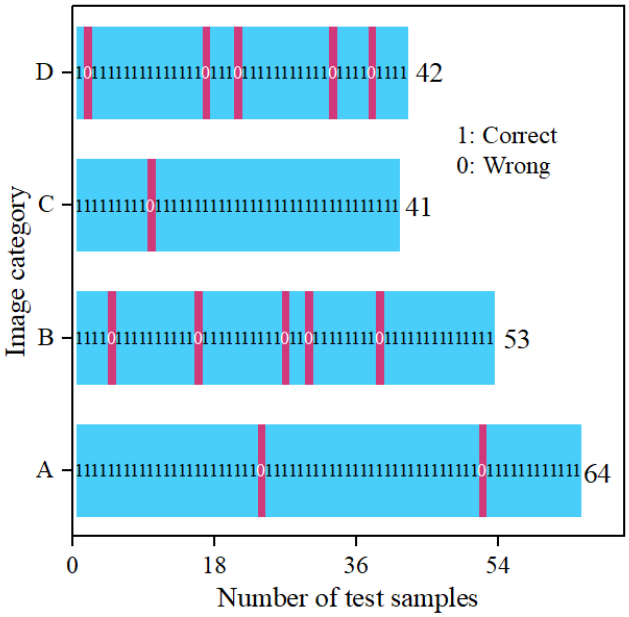

Figure 9: Statistical results of insulation fault detection

4 Conclusion

This paper combines adaptive morphological image segmentation technology to construct an intelligent detection model for power equipment driven by image segmentation algorithms, and analyzes the application effectiveness of the model in intelligent detection of power equipment.

The results show that the segmentation accuracy MIoU of the model in power equipment detection is 34.22% and 28.77% higher than that of the U-Net and DeeplabV3+ segmentation algorithms, respectively, and the detection accuracy of the image reaches 97.5%. Application cases demonstrate that the model achieves a true detection rate of 97.96% in the detection of corrosion faults in hardware and an average detection rate of 93.5% in the detection of damage faults in insulators, validating the effectiveness of the algorithm.

About the Authors

Xiaolong Chen, male, 2011- 2017, South China University of Technology, majoring in Electrical Engineering and Automation, Ph.D. During the Ph.D. program, he researched on the impact of DC system control on AC systems. 2006 -2009, Guangdong University of Technology, majoring in Power System and Automation, he focused on AI-based control for hybrid AC/DC transmission systems. Since 2009, working at China Southern Power Grid, a senior engineer, with 16 years experience at substation operation, he is a senior technical lead and in charges of smart operations and maintenance upgrade projects and management. As the first author, he has published 6 journal papers, 2 of which are indexed by EI.

Fang Luo, female, 2015-2018, South China University of Technology, majoring in Electric

Machines and Electric Apparatus, Master’s degree. She is an Engineer and a technician at China Southern Power Grid Co., As a pioneering contributor to the first wave of digital grid transformation, she spearheaded the advancement of remote intelligent operation and maintenance (O&M) for substations, conducting critical research on substation cybersecurity protection, equipment defect identification, and infrared-based device diagnostics.

Qiangchao Xu, male, 2003 - 2006, Huazhong University of Science and Technology, master of Engineering in Power System Automation. He focused on scheme design of substation monitoring systems for distribution network automation applications.2000 - 2003, Huazhong University of Science and Technology, Bachelor's degree. Since 2006, working at Guangzhou Power Supply Bureau, Guangdong Power Supply Co., Ltd., he is a Senior Engineer, specializing in operation, maintenance, and repair of relay protection and automation systems. As the first author, he has published 16 papers, 3 of which are indexed by EI.He has obtained 2 software copyrights and 38 patents in relay protection, and delivered notable innovations and practical applications in relay protection technology.

Yongbiao Liu, male, 2010-2012, Zhengzhou University, majoring in Electrical Engineering and Automation, Bachelor's Degree, his research focused on digital substation and applications. With 28-years professional experience in power substation field, he specializes in intelligent operation and maintenance, monitoring technologies, and substation operation management. As a principal creator, he directed the technical retrofit project "Remote Inspection & Operation Intelligent Upgrade of 110kV Jianfeng Substation, and awarded National Class II Innovation Achievement in Power Industry Equipment Management". He has participated in the research and construction of intelligent spatial management and intelligent operation and maintenance in the substation field of the Southern Power Grid.

Jilin He, male, 2012 - 2016, China Three Gorges University, majoring in Electrical Engineering and Automation, Bachelor's degree. During his undergraduate studies, he focused on intelligent operation and maintenance of substations. He comprehensively considered equipment inspection and temperature measurement, intelligent operation, and intelligent safety management and control at production sites, and adopted all effective intelligent methods to improve the operational efficiency of substations. Since 2016, he has been working at Guangzhou Power Supply Bureau Co., Ltd. as a First-Class Intelligent Operation and Maintenance Engineer. He has participated in intelligent transformation projects, realizing full coverage of intelligent operation and maintenance functions in newly commissioned incremental substations.

Zhaoqi Shi, male, 2021 - 2024, North China Electric Power University, majoring in Electrical Engineering, Master’s degree. 2017 - 2021, North China Electric Power University, majoring in Electrical Engineering and the Automation, Bachelor's degree. Since 2021, working at the Guangzhou Power Supply Bureau Substation Management Office of Guangdong Power Grid Co., Ltd., as a Senior Operator in the Relay Protection and Automation Department, responsible for the acceptance of multiple substation infrastructure and technical renovation projects, and responsible for the establishment of an innovation platform. Participated in the research and development and debugging of multiple technological innovation projects in the field of substation, and the achievements won the first prize of the Innovation Award for Employees of the China Electricity Council. Possess two invention patents related to the power field, both of which have been transformed into practical applications and are used in the working sites of the power industry.

References

[1] Li, S., & Li, J. (2017). Condition monitoring and diagnosis of power equipment: review

and prospective. High Voltage, 2(2), 82-91.

[2] Zhang, H., Su, B., & Meng, H. (2017). Development and implementation of a robotic inspection system for power substations. Industrial Robot: An International Journal, 44(3), 333-342.

[3] Jenssen, R., & Roverso, D. (2019). Intelligent monitoring and inspection of power line components powered by UAVs and deep learning. IEEE Power and energy technology systems journal, 6(1), 11-21.

[4] Lekidis, A., Anastasiadis, A. G., & Vokas, G. A. (2022). Electricity infrastructure inspection using AI and edge platform-based UAVs. Energy Reports, 8, 1394-1411.

[5] Chen, J., Jiang, J., & Zhu, B. (2022). Iot-based power detection equipment management and control system. Journal of Intelligent Systems, 31(1), 1229-1245.

[6] Jalil, B., Leone, G. R., Martinelli, M., Moroni, D., Pascali, M. A., & Berton, A. (2019). Fault detection in power equipment via an unmanned aerial system using multi modal data. Sensors, 19(13), 3014.

[7] Yang, C., Wu, X., Gong, W., Wang, Q., & Li, L. (2019). An intelligent identification algorithm for obtaining the state of power equipment in SIFT-based environments. International Journal of Performability Engineering, 15(9), 2382.

[8] Zhao, S., & Zhao, H. (2024). Intelligent Power Equipment for Autonomous Situational Awareness and Active Operation and Maintenance. Journal of Modern Power Systems and Clean Energy.

[9] Xingxin, C., Xin, Z., & Gangming, W. (2022). Research on online fault detection tool of substation equipment based on artificial intelligence. Journal of King Saud University-Science, 34(6), 102149.

[10] He, S., Zhang, Y., Zhu, R., & Tian, W. (2020). Electric signature detection and analysis for power equipment failure monitoring in smart grid. IEEE Transactions on Industrial Informatics, 17(6), 3739-3750.

[11] Yao, Z., Zhao, J., & Xue, D. (2023, November). Research on intelligent inspection system of substation. In International Conference on Internet of Things and Machine Learning (IoTML 2023) (Vol. 12937, pp. 123-127). SPIE.

[12] Zhang, Z., Wang, H., Chen, H., Shi, T., Song, Y., Han, X., & Li, J. (2023). A novel IEPE AE-vibration-temperature-combined intelligent sensor for defect detection of power equipment. IEEE Transactions on Instrumentation and Measurement, 72, 1-9.

[13] Roth, H. R., Shen, C., Oda, H., Oda, M., Hayashi, Y., Misawa, K., & Mori, K. (2018). Deep learning and its application to medical image segmentation. Medical Imaging Technology, 36(2), 63-71.

[14] Ghosh, S., Pal, A., Jaiswal, S., Santosh, K. C., Das, N., & Nasipuri, M. (2019). SegFast-V2: Semantic image segmentation with less parameters in deep learning for autonomous driving. International Journal of Machine Learning and Cybernetics, 10(11), 3145-3154.

[15] Johnson, B. A., & Ma, L. (2020). Image segmentation and object-based image analysis for environmental monitoring: Recent areas of interest, researchers' views on the future priorities. Remote Sensing, 12(11), 1772.

[16] Dorafshan, S., Thomas, R. J., & Maguire, M. (2018). Comparison of deep convolutional neural networks and edge detectors for image-based crack detection in concrete. Construction and Building Materials, 186, 1031-1045.

[17] Zheng, J., Gao, Y., Zhang, H., Lei, Y., & Zhang, J. (2022). OTSU multi-threshold image segmentation based on improved particle swarm algorithm. Applied sciences, 12(22), 11514.

[18] Ye, Q. (2021). Intelligent inspection system of power equipment based on photoelectric sensor/AR technology. Journal of Nanoelectronics and Optoelectronics, 16(10), 1645-1656.

[19] Ding, X., Gong, Y., Wang, C., & Zheng, Z. (2024). Artificial intelligence based abnormal detection system and method for wind power equipment. International Journal of Thermofluids, 21, 100569.

[20] Zhang, X., Lv, Z., Sun, Y., Huang, B., Niu, Z., Liu, G., & Mu, K. (2021, December). Intelligent detection technology of infrared image of substation equipment based on deep learning algorithm. In 2021 IEEE Sustainable Power and Energy Conference (iSPEC) (pp. 3855-3860). IEEE.

[21] Deng, F., Xie, Z., Mao, W., Li, B., Shan, Y., Wei, B., & Zeng, H. (2022). Research on edge intelligent recognition method oriented to transmission line insulator fault detection. International Journal of Electrical Power & Energy Systems, 139, 108054.

[22] Lu, W., Li, Q., Zhang, W., Mei, L., Cai, D., & Li, Z. (2024). Management of power equipment inspection informationization through intelligent unmanned aerial vehicles. Artificial Life and Robotics, 29(4), 579-584.

[23] Xuan, W., Li, Z., Chen, H., Peng, H., Guo, Y., Wang, X., ... & Wang, H. (2024, January). Exploration on Intelligent Detection Methods for Substation Equipment Based on Deep Learning. In 2024 IEEE 4th International Conference on Power, Electronics and Computer Applications (ICPECA) (pp. 332-335). IEEE.

[24] Shiling, Z., & Xiping, J. (2022, December). Image processing and deep learning technology help power equipment intelligent operation inspection. In 2022 12th International Conference on Power and Energy Systems (ICPES) (pp. 476-482). IEEE.

[25] Davari, N., Akbarizadeh, G., & Mashhour, E. (2021). Corona detection and power equipment classification based on GoogleNet-AlexNet: An accurate and intelligent defect detection model based on deep learning for power distribution lines. IEEE Transactions on Power Delivery, 37(4), 2766-2774.

[26] Wang, B., Dong, M., Ren, M., Wu, Z., Guo, C., Zhuang, T., ... & Xie, J. (2020). Automatic fault diagnosis of infrared insulator images based on image instance segmentation and temperature analysis. IEEE Transactions on Instrumentation and Measurement, 69(8), 5345-5355.

[27] Hong, C., Qiu, H. Y., Gao, J. H., Lin, S., & Guo, M. F. (2023). Semantic segmentation-based intelligent threshold-free feeder detection method for single-phase ground fault in distribution networks. IEEE Transactions on Instrumentation and Measurement, 73, 1-9.

[28] Duan, J., He, Y., Du, B., Ghandour, R. M. R., Wu, W., & Zhang, H. (2019). Intelligent localization of transformer internal degradations combining deep convolutional neural networks and image segmentation. IEEE Access, 7, 62705-62720.

[29] Zhang, J., & Zhu, W. (2023). Research on algorithm for improving infrared image defect segmentation of power equipment. Electronics, 12(7), 1588.

[30] Hou, Y., Xia, W., Liu, J., & Qi, Y. (2023, May). Lightweight DeepLabv3+ segmentation method for substation equipment oil leakage image. In 2023 4th International Conference on Mechatronics Technology and Intelligent Manufacturing (ICMTIM) (pp. 219-222). IEEE.

[31] Zou, W., Jiang, Y., Liao, W., Fan, S., Yang, Y., Hou, J., & Tang, H. (2025). Improved U-Net for Precise Gauge Dial Segmentation in Substation Inspection Systems: A Study on Enhancing Accuracy and Robustness. Information, 16(5), 382.

[32] Zhao, Z., Feng, S., Zhai, Y., Zhao, W., & Li, G. (2023). Infrared thermal image instance segmentation method for power substation equipment based on visual feature reasoning. IEEE Transactions on Instrumentation and Measurement, 72, 1-13.

[33] Fambrini, F., Iano, Y., Caetano, D. G., Rodriguez, A. A., Moya, C., Carrara, E., ... & Saito, J. H. (2018). GPU cuda JSEG segmentation algorithm associated with deep learning classifier for electrical network images identification. Procedia Computer Science, 126, 557-565.

[34] Qi, C., Li, Q., Liu, Y., Ni, J., Ma, R., & Xu, Z. (2020). Infrared image segmentation based on multi-information fused fuzzy clustering method for electrical equipment. International Journal of Advanced Robotic Systems, 17(2), 1729881420909600.

[35] Liu, X., Zhang, Z., Hao, Y., Zhao, H., & Yang, Y. (2024). Optimized OTSU segmentation algorithm-based temperature feature extraction method for infrared images of electrical equipment. Sensors, 24(4), 1126.

[36] Takeuchi, R. D. O. A., Ulbricht, L., Magrin, F. G. S., Ganacim, F. I. S., Fernandes, L. G., Romaneli, E. F. R., & Junior, J. U. (2022). Comparison of traditional image segmentation methods applied to thermograms of power substation equipment. Energies, 15(20), 7477.

[37] Kaihan Xiao,Qingshan Tang,Si Liu,Sijie Li,Jiayi Huang & Tao Huang. (2023). A novel dual-fusion algorithm of single image dehazing based on anisotropic diffusion and Gaussian filter. International Journal of Computational Science and Engineering, 26(1), 54-64.

[38] Suzhen Yuan,Xianli Li,Shuyin Xia,Xianrong Qing & Jermiah D. Deng. (2025). Quantum color image edge detection algorithm based on Sobel operator. Quantum Information Processing, 24(7), 195-195.